CHAPTER 2

Parametric Study of Normal Mode Frequencies and Cold-test Results

2.1 Introduction

A precisely designed modulation section is an essential requirement for reltron's decent performance. The modulation section consists of two on-axis pillbox cavities, and a side cavity, adjoining the first two. The side cavity facilitates inductive coupling. The reltron operates in $\pi/2$ mode. In addition to the operating mode, two normal modes resonate in the modulation section with nearby frequencies. The normal modes are designated depending on the phase difference of the EM fields in consecutive cavities. The mode frequencies depend on cavity dimensions. Proper tuning is necessary for optimum performance. Analytically finding the normal modes remains challenging due to complicated boundary conditions imposed by the structure's azimuthal asymmetry. Hence, the numerical technique based simulation software are employed.

The present chapter includes: i) design and working principle, ii) a parametric study of normal mode frequencies, and cavity optimization for equal and maximum mode separation, iii) obtaining S_{11} through simulation and calculation of quality factors along with cavity reactance in each mode, and iv) construction of a test cavity, and S_{11} measurement.

2.2 Concept of the Design

Reltron (Figure 2.1) has four independent sub-assemblies– beam injector, modulation cavity, post-accelerating gap region, and output extraction cavities.

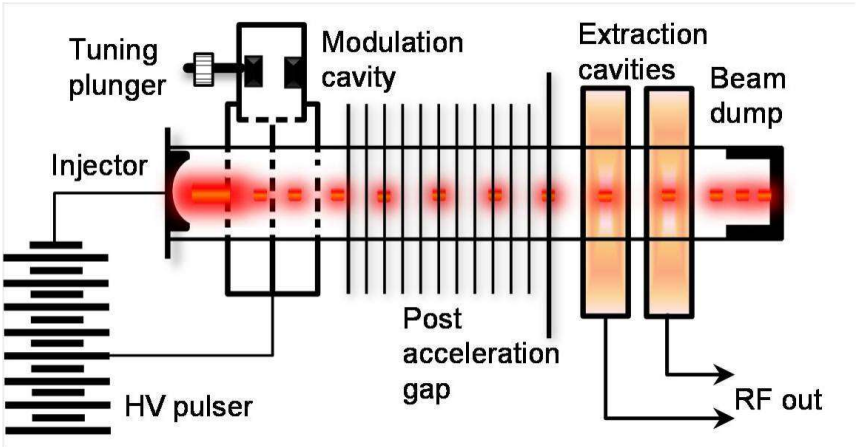

Figure 2.1: Schematic of reltron tube.

2.2.1 Beam injector

The schematic diagram of reltron is shown in Figure 2.1. Most of the high peak power gridded reltrons utilizes explosive emission type velvet cathodes that are suitable for long-pulse operation [Miller (1998)]. The velvet cathodes are cold cathodes that are inexpensive and require less technical expertise than the thermionic cathodes. However, these cathodes fail to operate at PRF greater than 10 Hz, and a pulse duration of more than 1 μS. Under these conditions, prolonged exposure of the grids to the electron beam makes the grid to melt at places. So, grid-less reltrons are used when high PRF and long pulse duration are required. The grids are replaced by metal discs with an aperture at the center for beam passage. Thermionic cathodes are employed in long pulse, high average power grid-less reltrons. They require small permanent magnets for beam focusing. The grid-less reltrons experimentally demonstrated a pulse duration of $\sim$5 μS and PRF of 100 Hz [Miller *et al.* 1995]. Output power and impedance as a function of diode voltage for both grid-less, and gridded reltrons has also been reported [Miller (1997)]. The glass-fibre cathode has been found more advantageous than velvet cathode. It has exhibited less

impedance depression towards the pulse end, and more reproducible operation [Smith *et al.* (2007)].

2.2.2 Modulation section

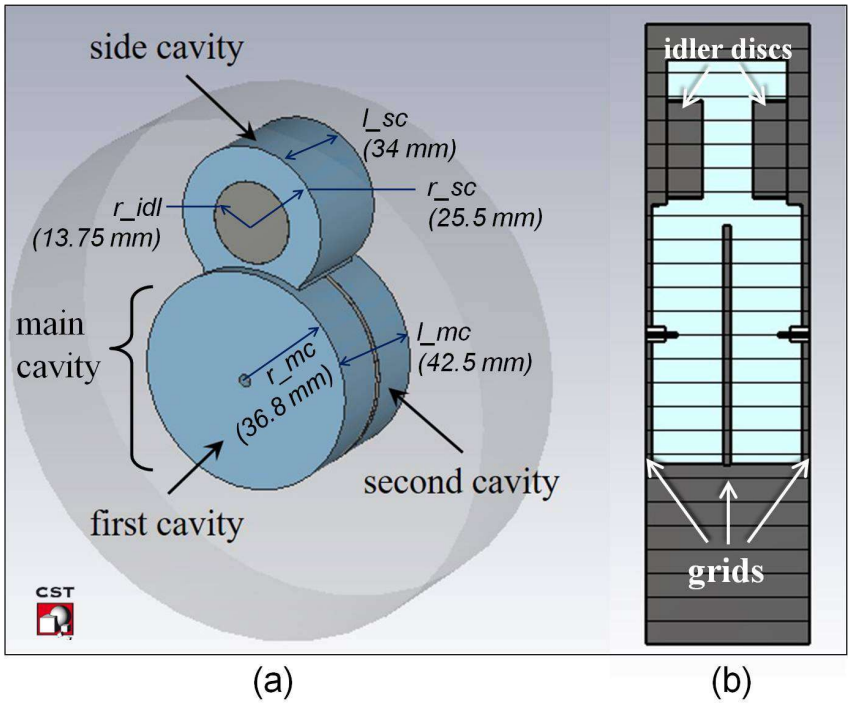

Figure 2.2: 3D model of gridded reltron's modulation section (a) perspective view, and (b) cross-sectional view.

Reltron's modulation section is comprised of the main cavity and a side cavity, as shown in Figure 2.2. The main cavity is a cylindrical pillbox * with two identical cavities. The side cavity is merged radially with the main cavity to facilitate RF coupling between the first two. Metallic idler discs are extended inside the cavity volume, making it a re-entrant cavity. Proper tuning of the idler discs creates the mode separation between 0 and $\pi/2$ modes, which subsequently results in optimum beam bunching. The main cavity end walls are made of grids (Figure 2.2(b)). The grids are woven from wires of stainless steel, molybdenum, or tungsten. Rectangular grids made of stainless steel 1 mil wire is woven 50 wires/inch in horizontal and vertical dimensions have been found suitable for low-frequency tubes. Highly transparent grids (circular shaped molybdenum grids with radial

*the cavity diameter is greater than its axial length

spoke, having 99% transparency) produced 400 nS pulse duration, but with lower output power. Higher beam modulation and faster conditioning resulted in using rectangular grids woven from 1 mil tungsten wires with 40 wires per inch [Miller (1998)].

The design of reltron's modulation section is similar to that of a single segment of side coupled LINAC with two half cells and one coupling cavity. When all three cavities are tuned to the same uncoupled resonant frequency, the $\pi/2$ mode characteristics remains identical to that for the periodic system [Knapp *et al.* (1968)]. The radius of constituents of the main cavity (r_mc) is calculated from the operating frequency in TM_{010} as

$$r\_mc = \frac{p_{np}}{2\pi f_{res}\sqrt{\mu_0 \varepsilon_0}}, \tag{2.1}$$

where $p_{np} = p_{01}$ = 2.405 is the p^{th} root of Bessel function J_n, and μ_0, and ε_0 are vacuum permeability, and permittivity, respectively. As the side cavity couples the first two, its inductance is twice of the individual cavities. In order to make the uncoupled resonant frequency of all three cavities equal, the capacitance of the side cavity must be halved [Soh *et al.* (2010)]. So, its radius (r_sc) is taken approximately two-third of the main cavity, since capacitance is proportional to square of the radius. Hence,

$$r\_sc = \frac{2}{3} r\_mc. \tag{2.2}$$

The radius and length of each idler disc are taken as

$$r\_idl = \frac{1}{2} r\_sc, \tag{2.3}$$

and

$$l\_idl = \frac{1}{3} r\_sc, \tag{2.4}$$

respectively. This design results in reasonably good mode separation. However, for having equal mode separation, the main cavity radius must be tuned further through horseshoe and idler tuning dials [Soh (2012)]. The design frequency should be kept $\sim$3% higher than the desired frequency of operation as the resonant frequency shifts in a coupled

multi-cavity structure. Also, the beam loading causes a minor reduction in the operation frequency [Gilmour (2011)]. The grid spacing (g) in the modulating section can be theoretically derived by assuming that an electron should cross the first (or the second) cavity in approximately one-half the oscillation period T. This argument gives

$$\frac{g}{v} = \frac{T}{2}, \quad \Rightarrow \quad g = \frac{v}{2f}, \tag{2.5}$$

where f is the frequency of RF field in $\pi/2$ mode, and v is the electron's velocity under the influence of applied DC potential V, given by

$$v = \sqrt{\frac{2eV}{m}}, \tag{2.6}$$

m being the mass of electron. The optimal grid spacing and anode-cathode gap distance (d_{ak}) have been optimized through several experimental observations as

$$g_{opt} = \frac{v}{3.2f}, \tag{2.7}$$

and

$$d_{ak} = 1.1g, \tag{2.8}$$

respectively. The drift tube radius is taken higher than the modulation section in order to keep its cutoff frequency lower than the modulation section. The drift tube's length is made few wavelengths long to ensure that the backward waves are attenuated. To maximize microwave power extraction from the longitudinally periodic current density peaks, which is a function of $cos(n\pi - k_z z)$ the drift tube length (z) must satisfy

$$l\_dt = \frac{n\pi}{k_z z}, \tag{2.9}$$

where n is an odd multiple of $\pi/2$, and $k_z = 2\pi/\lambda$ is the wavenumber. The length of

postacceleration gap (l_pa) is kept to be

$$l\_pa = l\_dt + \frac{h\_wg}{2}, \tag{2.10}$$

where h_wg is the height (along y axis) of extraction waveguide.

2.2.3 Postacceleration section

Reltrons utilize the postacceleration technique, which differentiates it from the klystrons. This results in higher output power as well as efficiency. A high DC potential is applied at the exit of the modulation section (Figure 2.1). This boosts the velocity of all the electrons to a mildly relativistic regime. Thus, the postacceleration supplies more kinetic energy to the beam that could be converted into RF energy. The postacceleration also reduces the kinetic spread that results in high efficiency. The peak efficiency without post-acceleration is about 20%, which doubles with postacceleration [Miller *et al.* (1992)].

2.2.4 Extraction section

Reltron's extraction section is constructed from standard rectangular waveguides. A waveguide is converted into a cavity by terminating its one end with a movable short. The other end has an inductive iris, whose opening is controllable. The power leaks out from the iris opening in TE_{10} mode and can be radiated without any mode converter. Multiple cavities can be used to extract RF power from the high energy electron beam. Output power from multiple cavities can be added in phase using a waveguide combiner section. Theoretical calculation of the reactance, the resonant frequency, and the shunt impedance of inductively loaded extraction cavity has been published [Miller *et al.* (1992)].

2.3 Working Principle

The working principle of reltron is briefly described here. An HV pulse drives the cathode, which emits a high current electron beam. While traversing through grids, the beam

interacts with all the normal modes inside the modulation section. The grids appear as infinitesimally thin foils that act like electrostatic lenses to focus the approaching beam [Fernsler *et al.* (1990)] and hence, an additional focusing arrangement is not required. Beam field interaction in $\pi/2$ mode results in a net energy transfer from beam to field. As a result, the field amplitude grows and results in current modulation. A steady-state is reached when there is no net energy transfer from beam to the field or vice versa. As the peak current becomes a significant fraction of space charge limiting current, virtual cathodes are formed periodically, resulting in dense bunching with a high relative kinetic spread. Postacceleration technique is used to enhance the beam kinetic energy, and to lower the kinetic spread. Iris loaded rectangular waveguide cavities extract the RF power from the post-accelerated beam as long as bunching persists. Finally, the spent beam is collected by an X-ray shielded beam dump. The operating frequency can be easily tuned by varying the cavity dimensions. With exchangeable extraction sections, power can be extracted from higher-order harmonics of the fundamental mode. The oscillation frequency is stable and does not suffer from mode competition or frequency chirping during normal operation.

2.4 Attractive Features

Reltrons are designed on the linear geometry of klystrons, which are one of the most reliable HPM sources [Benford *et al.* (2007)]. Klystrons suffer from a few inherent limitations. Multi cavity klystrons are considerably lengthy, and the requirement of beam focusing arrangement makes them bulky. Reltrons do not suffer from these limitations, and they have a few additional features–

Compactness: Reltrons utilize the $\pi/2$ mode, which is similar to fundamental SCO mode. This mode offers a large current modulation over a short distance [Marder *et al.* (1992)]. The $\pi/2$ mode segregates a relatively low energy electron beam into dense bunches within the modulation section, making reltron substantially compact. Also, it does not require is an additional mode converter, as power extraction in TE_{10} mode is more convenient for DEW applications. This helps the reltrons to remain compact.

Light-weight: The foil-focusing effect [Fernsler *et al.* (1990)] helps high peak power gridded reltrons operate without the need for a focusing structure, resulting in a drastic reduction in weight. However, the high average-power long pulse gridless reltrons require small permanent magnets for beam focusing.

High output power and efficiency: Application of the postacceleration potential plays a significant role in improving the output power, and efficiency. The high energy of the post-accelerated beam allows drawing off RF output from multiple extraction cavities.

Excellent frequency stability and tunability over a wide range: Reltron oscillates with relatively stable operating frequency since the bunching occurs due to beam field interaction in $\pi/2$ mode only. There is no chance of mode jumping since beam field interaction in other modes 0 and π do not lead to bunching. The operation frequency can be varied within 15% by symmetric tuning [Miller *et al.* (1998)].

Variable pulse duration and pulse repetition rate: With a wide variety of compatible power supplies, reltrons can operate with pulse duration from a few hundreds of nS to a unit of μS. Thermionic cathode based high average power gridless reltrons have demonstrated pulse duration of 5 μS, and PRF of up to 100 Hz [Miller *et al.* (1995)].

2.5 Mode Designation

In normal mode oscillation, all constituent cavities resonate at the same frequency. Any higher order mode can be explained as a linear combination of the normal modes. To obtain the EM field patterns and the frequencies of normal modes a 3D structure of the reltron modulation cavity is modeled in CST MWS and MAGIC. The boundary condition $E_{tangential} = 0$ is assigned to all the whole volume, and the structure is simulated using the Eigenmode solver, discussed in next sub-section. Three lower order normal modes called— 0, $\pi/2$, and π are found in the modulation section. These are spatial combinations of the dominant TM_{010} mode in each pillbox cavity. In TM_{010} mode, the electric field is maximum at the cavity axis along the beam passageway, and minimum near cavity side walls. The magnetic field is oriented in the transverse direction, and it is maximum at cavity side walls. Thus, TM_{010} mode is the most favorable for beam bunching due to

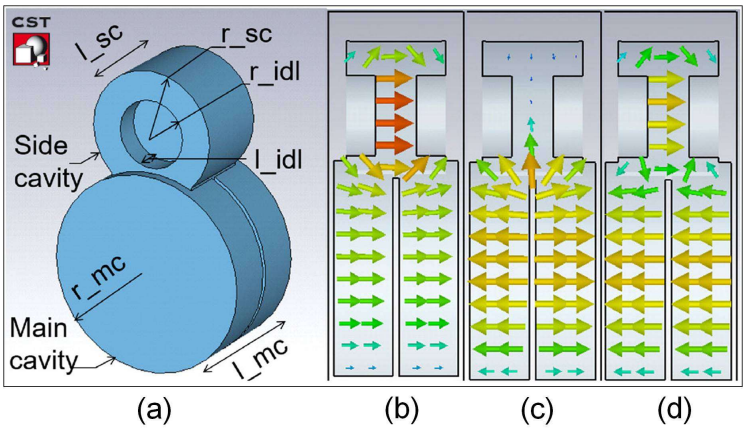

Figure 2.3: (a) Simulation model of the modulation section, and electric field vector-plots of (b) 0, (c) $\pi/2$, and (d)π mode, respectively [Miller *et al.* (1992)].

the maximum electric field at the cavity axis, and it facilitates magnetic coupling through the side cavity. This mode oscillates in the first, side, and second cavity in phase in 0 mode, and out of phase in π mode. Electric field vector plot of mode 0 and π mode are shown in Figures 2.3 (b), and (d), respectively. In addition to these modes, the composite arrangement of the three partially merged cavities gives rise to a new mode, called $\pi/2$ mode. In this mode, the electric field is out of phase in the first and the second cavity, and there is a negligibly small field in the side cavity, as shown in Figure 2.3 (c). MAGIC code is also used to obtain and compare the EM field patterns and frequencies of the three modes. Both the software produced similar field patterns with a small difference in oscillation frequency. Figure 2.4 shows the electric field vector plot and contour plot of the same. A comparison between the two software packages are given in Table 2.1.

Table 2.1: Comparison of normal mode frequencies (GHz) between MAGIC, and CST (Eigenmode)

Mode	MAGIC	CST (Eigenmode)	Difference (%)
0	2.8043	2.7175	3
$\pi/2$	3.0311	2.9147	3.8
π	3.1485	3.1090	1.3

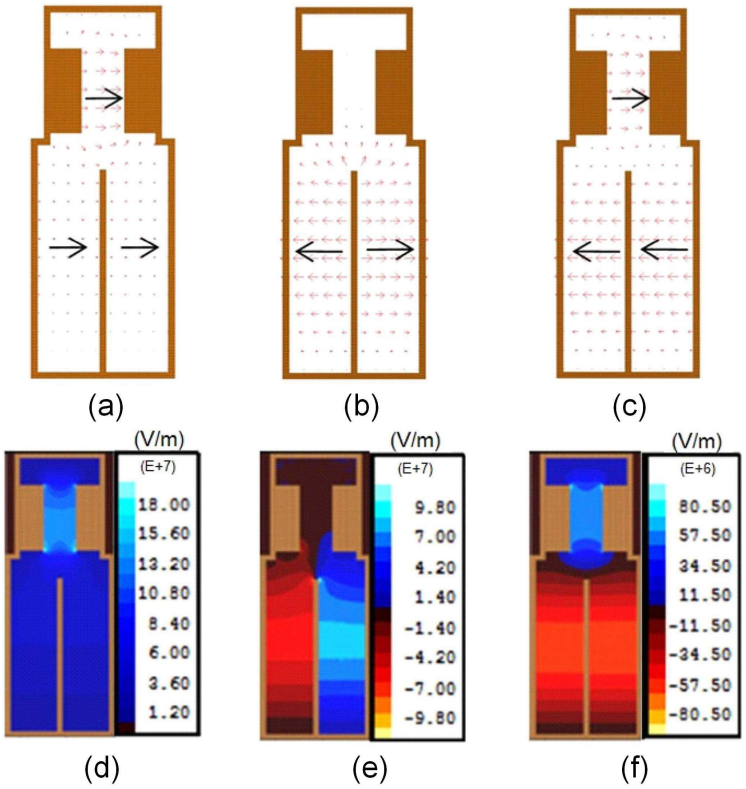

Figure 2.4: (a), (b), and (c) electric field vector plot in 0, $\pi/2$ and π modes; (d), (e), and (f) contour plots of the respective modes in reltron modulation cavity using MAGIC.

2.5.1 Eigenmode solver

The Eigenmode solver is used for finding the normal modes. The methods and algorithms of CST MWS, and MAGIC are summarized below.

CST MWS: The Eigenmode solver in CST MWS evaluates EM field equations inside the designed volume and finds all possible solutions considering the applied bounded conditions. Depending on the problem type, any one of the two methods, namely the Advanced Krylov Subspace method (AKS) or the Jacobi-Davidson method (JDM), can be chosen when hexahedral meshing is used in CST MWS. The AKS method finds the specified numbers of lowest order eigenmodes considering the lossless condition. This method has been utilized here. The JDM method can automatically choose the number of modes within the given frequency range, or it can find the specified numbers of mode above certain given frequency. The JDM method can take losses into consideration, and it is suitable when few modes are required, or degenerate modes are concerned. It consumes

more computational resources and requires more time.

MAGIC: The EIGENMODE command gives an eigenvalue solution of the Maxwell's equations in time domain. The command is applicable to any 2D or 3D geometry of non-lossy elements, and no source or sinks are permitted. The initial run should use '[SCAN_AT frequency]' (zero by default), which finds the lowest mode of a system. Other command arguments– 'SCAN_FROM', 'SCAN_TO', and 'SCAN_LIST' can be used according to the problem type. The modes can be searched by specifying an 'WINDOW'. If several eigenmodes appear within the frequency window, the mode closest to the center frequency will dominate, but it may have some contamination from the nearby mode. Thus, the frequency window should not be wider than the spacing between modes. The computational time increases as the width of the frequency window is made narrower. Here, the command and the arguments are used as 'EIGENMODE SCAN_FROM 2.6 GHz SCAN_TO 3.2 GHz WINDOW 100 MHz;'. The 'FORCE_TO_ZERO' option permits the user to force the zeroing of some field components resulting is a purer mode. This is useful when looking for a particular mode, in which one or more components of **E** or **B** are identically zero.

2.6 Parametric study of Normal Mode Frequencies

The normal modes 0, $\pi/2$, and π have close frequencies in increasing order. It is understood that the resonant frequencies in a single, and uncoupled cavity would follow an inverse relationship with cavity dimensions. But, in a coupled cavity structure like reltron's modulation section, relations among the normal modes frequencies and the dimensional parameters are unclear. To study the effect of cavity dimensions on the resonant mode frequencies, an S-band reltron modulation section is designed and modeled in C-ST MWS, and simulated in AKS method to obtain the three lower order normal modes. The field patterns of simulated mode 1, 2, and 3 agree with that of 0, $\pi/2$, and π mode, respectively. Thereafter, the post-processing tool is used for simultaneous monitoring of the three modes. Now, the parameters are varied sequentially over the range within which these three modes do not change their order, and no higher order modes appear near π

mode. In the process, the optimum cavity dimensions for equal and maximum separation between the three modes has been noted. Figure 2.5 (a)-(g) shows the variation of mode frequencies in parameter space over which the change is notable. The results are discussed in details in the conclusion of this chapter. Cavity dimensions that result in equal and maximum mode separation are listed in Table 2.2.

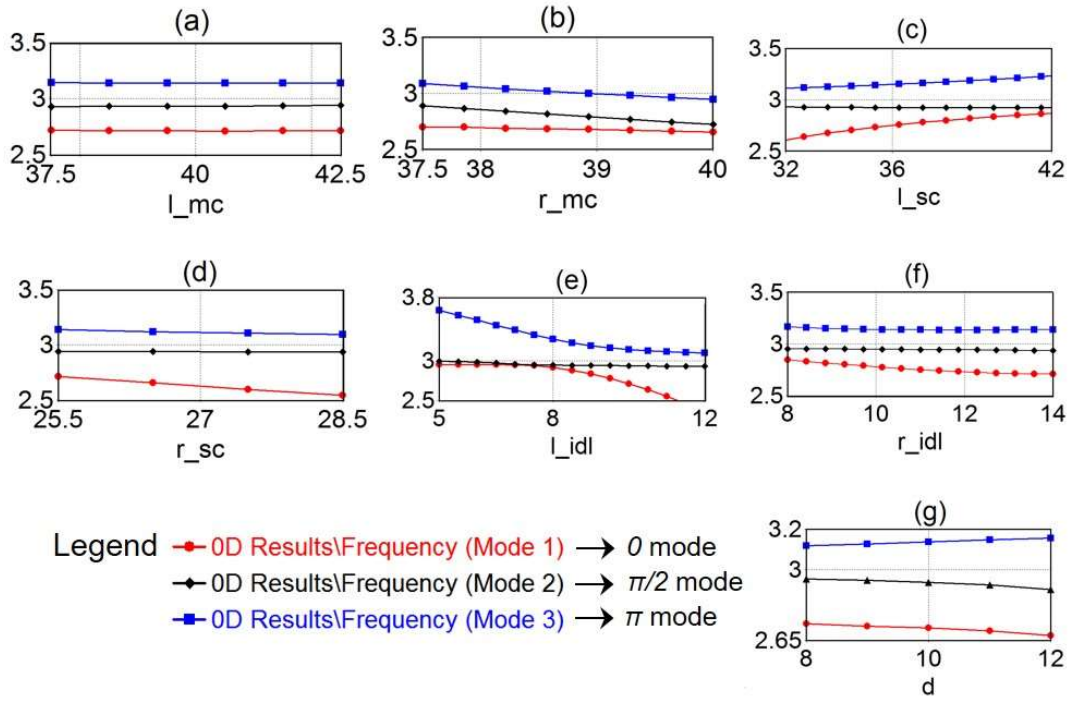

Figure 2.5: Frequencies of resonant mode (GHz) vs. cavity dimension (mm) – (a) length of main cavity, (b) radius of main cavity radius, (c) length of side cavity, (d) radius of side cavity, (e) length of idler disc, (f) radius of idler disc, and (g) depth of coupling.

2.7 Simulation of S-parameter

The normal mode frequencies can accurately be predicted by simulation, but there is no way of direct measurement. However, the S_{11} can be obtained through simulation and measurement. From S_{11}, the quality factor and cavity reactance can also be calculated. To obtain the S_{11} of the modulation section, standard flange-mount SMA connector is modeled along the cavity axis. Choi *et al.* have reported a similar experimental work, where end stripped coaxial cable was used to excite TM_{01} mode inside the cavity. In this simulation model, the modulation section is enclosed by a cylindrical volume of a perfect

Table 2.2: Dimensions of the modulation cavity for maximum mode separation.

List of parameters	Values (mm)
Main cavity length (l_mc)	42.5
Main cavity radius (r_mc)	36.8
Side cavity length (l_sc)	34
Side cavity radius (r_sc)	25.5
Idler disc length (l_idl)	10
Idler disc radius (r_idl)	13.75
Coupling depth (d)	10
Grid thickness (ŧ)	2

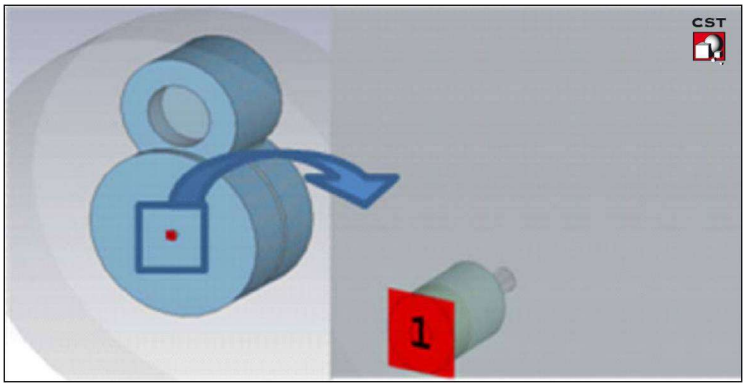

Figure 2.6: An enlarged view of waveguide port on SMA connector for obtaining S_{11}.

electric conductor (PEC) that represent the metallic walls. Hence, the outer conductor of the SMA connector is not modeled separately. Teflon (ε_r = 2.1, loss-free) is used as the dielectric material. It is excited by waveguide port as shown in Figure 2.6. The model is simulated using Frequency-domain solver and the result is shown in Figure 2.7. Three distinct minima at frequency 2.7, 2.9, and 3.1 GHz have been obtained that implies the frequency selective, and resonant behavior of the modulation section. The Eigenmode solver predicts that the three resonant modes can sustain oscillation inside the cavity. The S_{11} obtained from the Frequency-domain solver indicates that waves with almost the same frequencies may propagate through the cavity with minimum reflection. Table 2.3 shows the close convergence of the normal mode frequencies and that of the S_{11} minima.

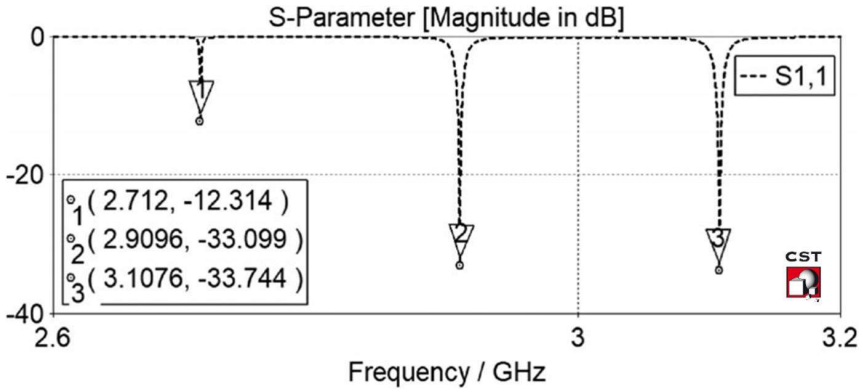

Figure 2.7: Simulated S-parameter of reltron modulation section. Marker 1, 2 and 3 correspond to 0, $\pi/2$, and π mode, respectively.

Table 2.3: Comparison of normal mode frequencies (GHz), and that of S_{11} minima.

Mode	CST (Eigenmode)	CST (Freq. dom.)	Difference (%)
0	2.7175	2.7120	0.20
$\pi/2$	2.9147	2.9096	0.17
π	3.1090	3.1076	0.05

2.7.1 Frequency-domain solver

The S-parameters show the frequency domain representation of RF energy propagation through any multi-port network in terms of reflection and transmission characteristics. In general, Maxwell's equations have to be transformed into the frequency domain, and the simultaneous equations have to be solved at every frequency samples within the frequency band of interest. In the general-purpose broadband frequency sweep method of the Frequency-domain solver of CST MWS, a fewer number of frequency samples drive a full broadband spectrum. This solver is suitable for fast calculation of S-parameter for strongly resonating structures like filters and resonant cavities. However, the scope of this solver is limited in handling large structures, as it becomes memory intensive and slow in solving the matrix equations in the increased number of mesh cells. Also, it can not handle structures containing nonlinear devices like diodes.

2.8 Calculation of Quality-factor and Cavity Reactance

Quality factors (Q) and cavity reactance can be calculated in each mode from S_{11} data [Khanna *et al.* (1983)]. The Loaded Q (Q_l) is calculated from

$$Q_l = \frac{f_0}{\Delta f}, \tag{2.11}$$

where f_0 is the resonant frequency, and Δf is half power bandwidth. The Δf is obtained in each mode by setting a horizontal marking line at -3 dB that cuts the S_{11} at two points, and measuring the interval by two vertical measure lines. The unloaded Q (Q_0) and the external Q (Q_{ext}) are subsequently calculated from

$$Q_0 = (1 + \boldsymbol{\beta})\, Q_l, \tag{2.12}$$

and

$$Q_{ext} = \frac{Q_0}{\boldsymbol{\beta}}, \tag{2.13}$$

respectively. Here $\boldsymbol{\beta}$ is the VSWR at resonance. To find out the VSWR, the locus of S_{11} is traced on impedance Smith chart. This gives the complex impedance at the three frequencies as shown in Figure 2.8. The reflection coefficient (Γ) and VSWR are calculated. The quality factors satisfy Equation (2.14) for all three resonant modes.

$$\frac{1}{Q_l} = \frac{1}{Q_0} + \frac{1}{Q_{ext}} \tag{2.14}$$

Assuming the parallel LC equivalent model of the cavity resonator (Figure 2.9), the quality factor can be expressed as

$$Q_l = \frac{B}{G} = \frac{1/\omega L}{1/R_{eq}} \;\; or \;\; \frac{1/\frac{1}{\omega C}}{1/R_{eq}} \tag{2.15}$$

where R_{eq} is the equivalent resistance of the two ports (50$\|$50=25 ohm) and G and B

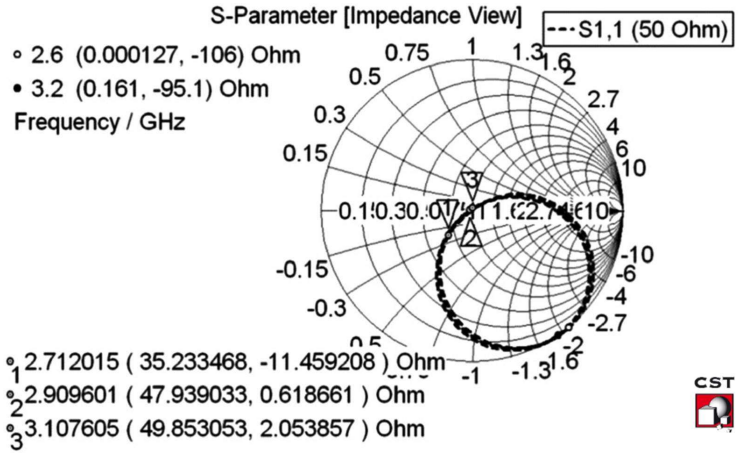

Figure 2.8: Impedance locus of S_{11}. Marker 1, 2, and 3 correspond to complex impedance in 0, $\pi/2$, and π mode, respectively.

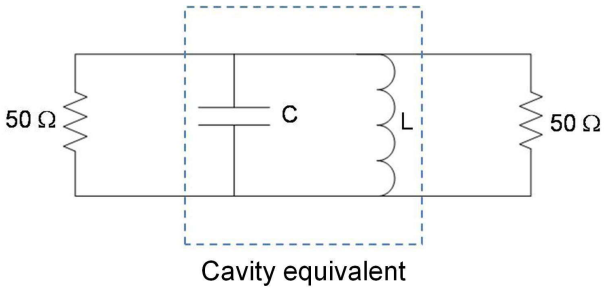

Figure 2.9: Equivalent model of reltron cavity for obtaining cavity reactance.

are the conductance and susceptance respectively. So, L and C can be calculated from [Collin (2007)]

$$L = \frac{R_{eq}}{\omega Q_l}, \quad and \quad C = \frac{Q_l}{\omega R_{eq}}, \tag{2.16}$$

when Q_l is known. The reflection and coupling coefficients, quality factors, inductance and capacitance in individual modes are summarized in Table 2.4.

Table 2.4: Quality factors, inductance and capacitance of the cavity in respective modes

Mode	Refl. Coeff. (Γ)	VSWR (β)	Q_l	Q_0	Q_{ext}	L (pH)	C (nF)
0	$-$ 0.15 $-$ j 0.15	1.55	1567	4005	2575	0.94	3.68
$\pi/2$	$-$ 0.02 + j 0.006	1.04	288	588	563	4.75	0.63
π	$-$ 0.001 $-$ j 0.02	1.04	257	525	504	4.99	0.52

2.9 Construction of a Test-cavity and S_{11} Measurement

The parts were built, and assembled to construct a test-cavity, and S_{11} was measured.

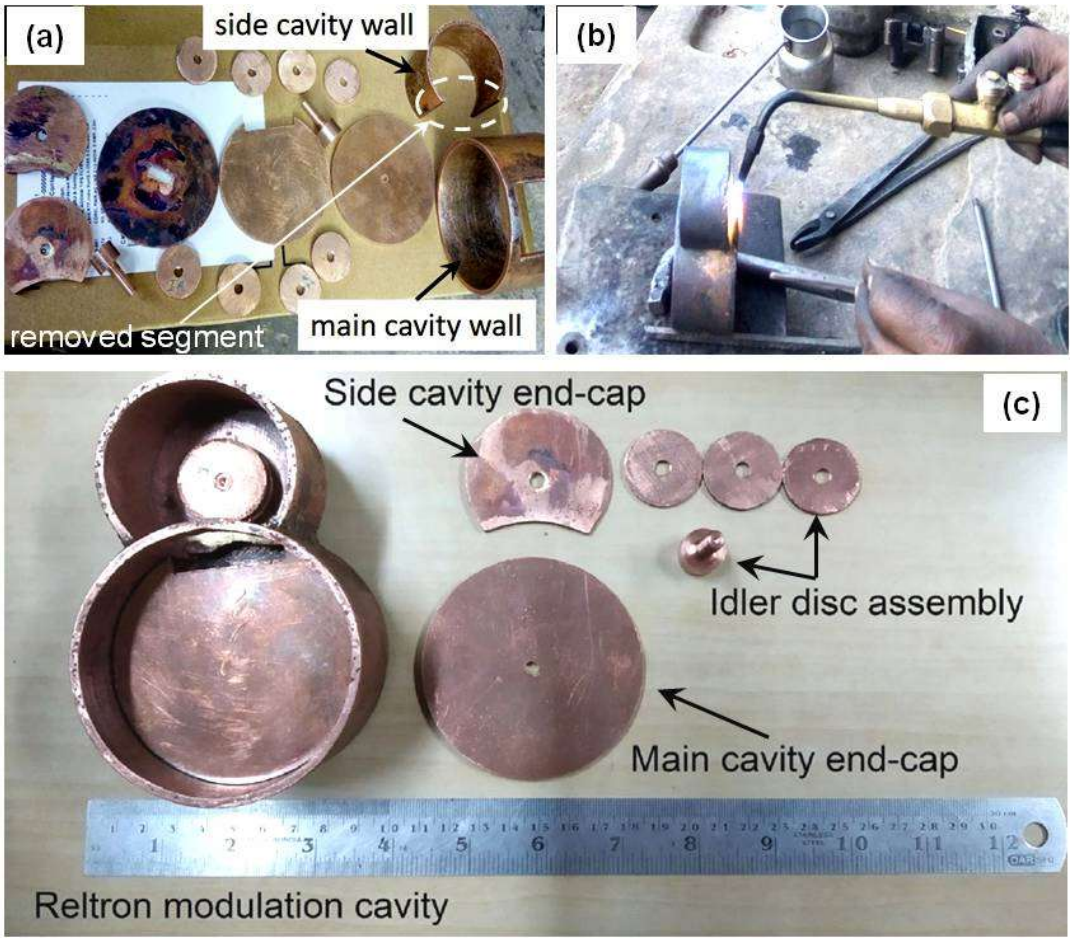

Figure 2.10: Construction of reltron modulation section showing– (a) different parts of the cavity, (b) the main cavity being joined with the side cavity by gas welding, and (c) final structure.

2.9.1 Construction of test-cavity

Different parts of a reltron's modulation section with the dimensions listed in Table 2.2 were constructed from a high purity electrical grade copper sheet. Though, the required sheet thickness was 2 mm, an 11 gauge (2.946 mm) sheet was procured to keep an error margin. It was machined to the exact thickness when required. For constructing the cylindrical walls of the main and the side cavity, rectangular parts with length equal to the corresponding cavity circumference, and width equal to the cavity height were cut from

the sheet using a shearing machine. The parts were bent using press break machine, and final cylindrical shape given by wooden mallet. The two cylinders were gas welded using high copper-alloy filler rod, after removing a segment from the side cavity cylinder and cutting a slot in the main cavity cylinder that matches properly with the segment (Figure 2.10 (a), (b)). The two idler disc assemblies were built by mounting six circular discs on two threaded bolts. The bolts were machined from a solid copper rod and threads were cut. The discs and the cavity end-caps were precisely cut from the main sheet by Computerized Numerical Control (CNC) machine. Each disc was drilled at the center and threaded to fit the bolt. One side of the cavity has been closed by the end-caps and welded permanently. The other side is kept open for altering the idler disc parameters in future studies. The end-caps were tightly fitted in the cavity opening and joined with the side walls using aluminum tape (inset Figure 2.11 (a)). Electrical continuity was verified using a volt-ohm-multi-meter (VOM) for ensuring the entire cavity volume is enclosed by a single conducting boundary. Solid discs were used instead of grids as the boundary conditions are similar in both the cases. The construction and assembly of reltron are relatively easy in comparison to helical or functionally tapered structures, used in TWTs and BWOs. The parts can be manufactured with high precision by CNC machine.

2.9.2 Cold-test results

Standard SMA connectors with exposed TFE (Tetra-fluoro Ethylene) were soldered along the axis of the main cavity end-caps to connect the VNA port. It was calibrated for S_{11} measurement. The measurement setup is shown in Figure 2.11 (a). The VNA port 1 was connected to the permanently welded side of the cavity. Anritsu MS2037C VNA was used to measure the S_{11}. The measured S_{11} is shown in Figure 2.11 (b). Three distinct minima were obtained as predicted through simulation. Table 2.5 lists the frequencies of S_{11} minima obtained by simulation and measurement. The simulated and the experimental results are combined in Figure 2.12

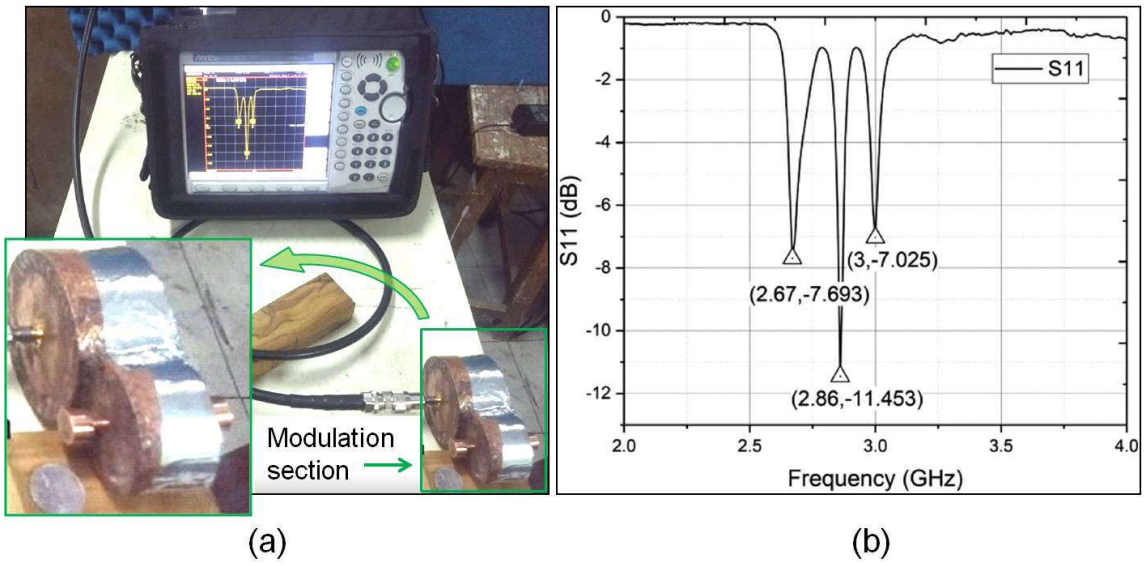

Figure 2.11: (a) Experimental set-up, and (b) measured S_{11}.

Table 2.5: Frequencies (GHz) of measured, and simulated S_{11} minima.

Mode	Measured S_{11}	Simulated S_{11}	Difference (%)
0	2.6700	2.7120	1.6
$\pi/2$	2.8599	2.9096	1.7
π	3.0000	3.1076	3.5

2.10 Conclusion

The chapter concludes the following – i) The Eigenmode solver obtains the three resonant modes, which can sustain oscillation inside the cavity, subjected to appropriate boundary conditions. The S_{11} from the Frequency-domain solver reveals that the waves with same frequencies as the normal modes may propagate through the cavity with minimum reflection. The measured S_{11} indicates that the operating mode $\pi/2$ may traverse the structure with least reflection among the three.

ii) The MAGIC and CST MWS Eigenmode solver produced similar EM field patterns but, a frequency difference of 1.3-3.8% was found. One possible reason for this difference is the unlike meshing techniques in the finite integration technique (FIT) based CST MWS, and the finite-difference time-domain (FDTD) based MAGIC. For Eigenmode and Frequency-domain solver of CST MWS, the mode frequency differed by less than 0.2%.

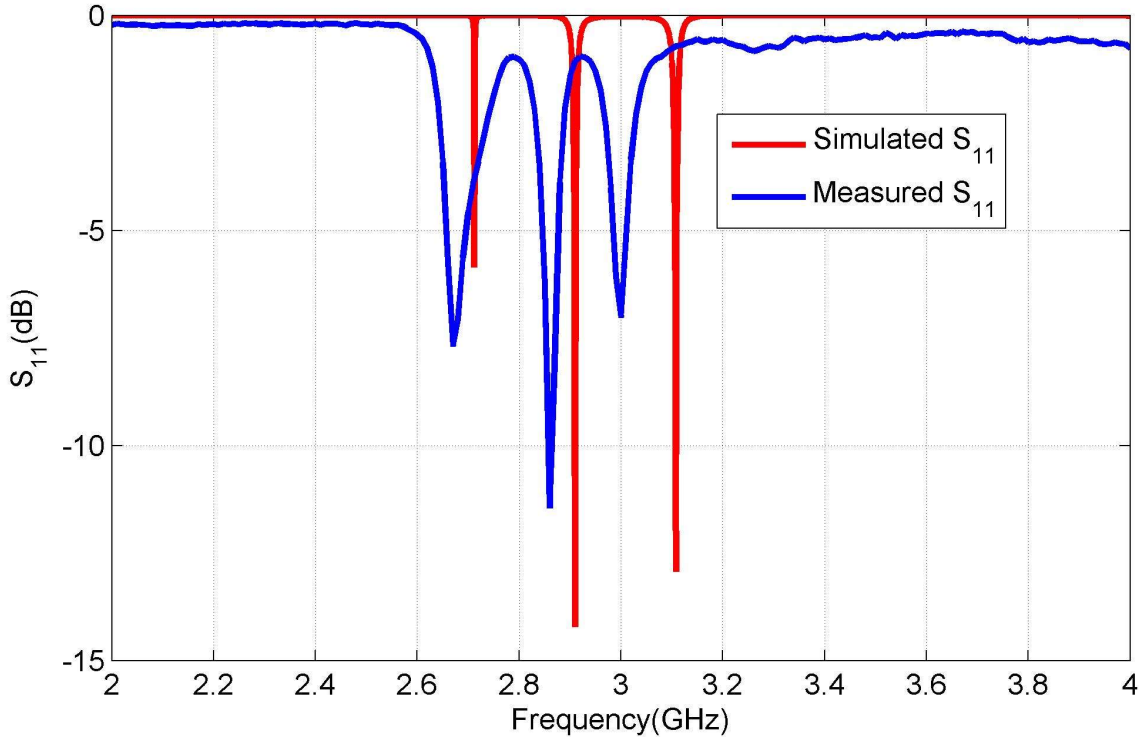

Figure 2.12: Combined picture of simulated and measured S_{11}.

In the case of simulated and measured frequencies of S_{11} minima, fairly good agreement has been found. However, slight variation was found. Considering the human error involved in constructing the test-cavity parts, and the subsequent difference between the ideal simulation model and constructed cavity, this is acceptable. The difference in the dB level between the experimental and the simulated result is due to losses in the practical measurement set-up.

iii) The parametric study concludes that three parameters control the frequency and mode separation. The main cavity radius (r_mc), and the coupling depth (d) govern the operating frequency. The idler disc length (l_idl) governs both the mode separation as well as the operating frequency. The parametric study results are summarized in Table 2.6, and it is valid for all frequency bands as the cavity dimensions scales inversely with frequency.

iv) Calculating the cavity reactance is important for any microwave tube for considering the beam loading. A fairly simple way of calculation has been presented.

v) MAGIC code failed to obtain mode 0 in earlier reported work [Soh *et al.* (2010)]. To successfully captures all three modes using MAGIC, a full 3D modeling of the cavity structure has been used. Further, in EIGENMODE command, we specified the frequen-

Table 2.6: Summary of change in resonant mode frequencies with cavity parameters.

Dimension of Cavity Parameters ↑		Frequency of mode† 0	$\pi/2$	π
Main cavity	length (l_mc)	–	–	–
	radius (r_mc)	↓	↓	↓
Side cavity	length (l_sc)	↑	–	↑
	radius (r_sc)	↓	–	↓
Idler disc	length (l_idl)	↓	–	↓
	radius (r_idl)	↓	–	–
Coupling depth	(d)	↓	↓	↑

†Table 2.6 ↑ increase, ↓ decrease, – no change.

cy range of 2.6 to 3.2 GHz, with prior knowledge of mode frequencies from CST MWS simulation with a specified window of 100 MHz.